Materials Science and Engineering C 70 (2017) 15–20

Contents lists available at ScienceDirect

Materials Science and Engineering C

journal homepage: www.elsevier.com/locate/msec

Nanostructured screen-printed electrodes based on titanate nanowires for biosensing applications

Helen Conceição Ferraz *, Daniela Ferreira Machado, Neuman Solange de Resende

Programa de Engenharia Química, COPPE – Universidade Federal do Rio de Janeiro, P.O. Box 68502, Rio de Janeiro, RJ 21941-914, Brazil

ARTICLE INFO

Article history:
Received 20 May 2016
Received in revised form 27 July 2016
Accepted 18 August 2016
Available online 20 August 2016

Keywords:
Screen-printed electrode
Titanate nanowires
Biosensor
Hydrogen peroxide
Horseradish peroxidase
Enzyme immobilization

ABSTRACT

This work demonstrates the successful modification of screen-printed electrodes using functionalized titanate nanowires for producing a peroxide biosensor. Titanate nanowires were synthesized by the hydrothermal method and characterized using physico-chemical techniques. The surface of the nanowires was modified with (3-aminopropyl)trimethoxysilane and glutaraldehyde to immobilize horseradish peroxidase through covalent bound, obtaining a surface coverage of 1.62 mg of enzyme/m^2. The surface of screen-printed carbon electrodes was modified with peroxidase-containing nanowires. Cyclic voltammetry and chronoamperometry were employed to study the electrochemical properties of the nanostructured electrode. A low hydrogen peroxide reduction potential around −0.98 V (*vs* Ag, pH 7.0) was observed, with linear response in the range of 40 to 560 μmol L^{-1}, detection limit of 10.7 μmol L^{-1} and good stability. Reproducibility relative standard deviation was as low as 4.7%. For repeatability, deviation was 3.3%.

1. Introduction

The global market for biosensing devices was over US$ 13 billion in 2013, with projection of a growth mainly driven by their application in medical diagnostics, in addition to the environmental monitoring field [1]. The quantification of hydrogen peroxide (H_2O_2) has drawn particular interest due to the great importance of peroxide in clinical and environmental applications and in mining, textile and food industries [2–5].

Devices based on enzymes immobilized on nanomaterials have proven high sensitivity to H_2O_2. Metal, carbon or polymer nanomaterials can be used to develop biosensors with high sensitivity and stability. Their excellent conductivity increases the electron transfer between the protein redox center and the electrode surface. Because of their high surface-volume ratio and enhanced electrons transport, their electrical properties are very sensible to minimal changes in the system [6–9]. These properties provide fastness and sensitivity to biosensors for direct electron detection [10–11]. Due to the biocompatibility, lower detection limits can be achieved and the detection potential is close to the enzyme redox potential, minimizing interfering reactions [11–12].

Various types of enzyme biosensors based on nanomaterials have been reported [13–17]. Studies have shown that modification of electrodes with titanate nanostructures can increase the direct transport of electrons *via* surface reactions [18–22].

Table 1 shows a comparison of nanostructured biosensors reported in the literature for H_2O_2 detection. In our previous work [23] we developed a biosensor for H_2O_2 using HRP immobilized on titanate nanowires surface. The fabricated biosensor exhibited a low reduction potential (around −0.38 V *vs* Ag/AgCl at pH 7.0), electrons transfer rate of 3.5 s^{-1}, linear range of 250 to 6.760 μmol L^{-1} and a detection limit of 1.2 μmol L^{-1}. In that work, an electrochemical stirred cell was used as biosensor platform.

For biosensing applications, other important characteristics are simplicity, robustness and portability. Regarding this matter, the development of screen-printed electrodes has met this demand, offering a complete system of electrodes designed with great simplicity and economy [28–29]. Some studies on the modification of screen-printed electrodes through HRP deposition reported low detection limit of hydrogen peroxide [30–31]. Immobilization of HRP on gold (nano)particles [32–33] or graphene structures [34–35] are strategies adopted to improve the biosensor performance in terms of detection limit and linear range. This work aimed at the modification of screen-printed electrodes through the deposition of HRP immobilized onto titanate nanowires.

2. Experimental

2.1. Materials

Horseradish peroxidase type IV (HRP, MM 44 kDa, RZ 3.0), bovine serum albumin (BSA), (3-aminopropyl)trimethoxysilane (APTMS, 97%) and hydrogen peroxide (H_2O_2, 30% *w*/*w*) were supplied by Sigma-Aldrich (St. Louis, MO, USA). Glutaraldehyde ($C_5H_8O_2$, 25%), sodium hydroxide [NaOH (PA)], nitric acid [HNO_3, 65% (PA)] and

* Corresponding author.
E-mail address: helen@peq.coppe.ufrj.br (H.C. Ferraz).

http://dx.doi.org/10.1016/j.msec.2016.08.046
0928-4931/

Table 1
H_2O_2 biosensors based on titanate nanostructures.

Biosensor	E (V *vs* Ag/AgCl)	Linear range (μmol L^{-1})	Detection limit (μmol L^{-1})	Reference
TNW/CHIT/GOx	0.60	10–6980	10.0	[24]
TNT/HRP	−0.50	11–2000	1.2	[20]
TNT/Au/HRP	−0.40	5–1000	2.1	[25]
TNW/HRP	−0.38	250–6760	1.2	[23]
TNT/Hb	−0.24	0.5–100	0.1	[26]
TNT/GOx	−0.10	15–4000	5.0	[27]

TNW – titanate nanowires; TNT – titanate nanotubes; CHIT – Chitosan; GOx – glucose oxidase; Hb – Hemoglobin.

dichloromethane (CH_2Cl_2, 99.5%) were purchased from Vetec-Sigma (Rio de Janeiro, Brazil).

2.2. Synthesis and characterization of titanate nanowires

Titanate nanowires (TNW) were synthesized by hydrothermally processing the titania (TiO_2, anatase) powder with 10 mol L^{-1} NaOH solution. The temperature was raised at a heating rate of 10 °C/min from room temperature to 130 °C [36]. The final temperature (130 °C) was held constant for 24 h. After cooling overnight under stirring, the product was filtered and rinsed with 1 M HNO_3 to obtain sodium-free TNW. After a final wash with distilled water to lower pH to 7.0, nanowires were dried overnight at 100 °C.

TNW morphology, composition and textural properties were characterized using field-emission scanning electron microscopy (FEG/SEM) (FEI Company Quanta 200), powder X-ray diffraction (XRD) analysis (Rigaku Miniflex equipment with CuKα radiation, λ = 15,418 Å), semi-quantitative powder X-ray fluorescence (XRF) analysis (Rigaku RIX 3100, with Rd tube, 4 kW), Raman spectroscopy (LabRam Horiba HR-800 UV-resolution 1 μm^3, with He—Ne laser – wavelength 632 nm) and N_2 physisorption (77 K, ASAP 2020 Micromeritics instrument, with pretreatment under vacuum at 573 K for 12 h). Specific surface was calculated by using the classic BET equation in the P/Po range of 0.06–0.21.

2.3. Immobilization of HRP on TNW

HRP immobilization through covalent bond was carried out according to previously described procedure [23]. Briefly, after treatment with APTMS and glutaraldehyde, 1 mL of 1 mg·mL^{-1} HRP solution in 0.1 mol L^{-1} phosphate buffer (PB) was added to 10 mg of functionalized TNW under stirring, for 2 h, at room temperature. Non-bound HRP was separated using 100 kDa Amicon filters under centrifugation.

The amount of immobilized HRP was quantified using Bradford assay from the difference between the protein concentration in solution before and after adsorption. Specific enzymatic activity (U/mg) was determined by spectrophotometry using an oxidative reaction catalyzed by HRP. In this case, hydrogen peroxide reacts with 4-aminoantipyrine forming the complex quinoneimine, which is detected at 510 nm. Immobilization efficiency was evaluated by infrared analysis (FTIR) (Perkin Elmer, Spectrum 100).

2.4. Modification of screen-printed electrodes

Screen-printed electrodes (IS-1 Florence sensors) with graphite as working electrode (3 mm in diameter, 0.071 cm^2 of area) were modified by deposition of HRP-containing TNW. The reference and counter-electrodes were made of silver paste (E_0 = 0.799 mV) and carbon past, respectively. For modification, 30 μL of TNW suspension in PB 0.1 mol L^{-1} pH 7.0, was dropped onto the working electrode surface. After drying, 30 μL of a 10% alcoholic solution of Nafion® was used to cover the electrode surface. When not in use, the modified electrode was stored in 0.1 mol L^{-1} PB pH 7.0 at 4 °C.

Electrochemical measurements were conducted using a PalmSens® workstation. Cyclic voltammetric (CV) analysis of the biosensor were performed at room temperature (23 °C) in the presence of 0.1 mol L^{-1} KCl in 0.1 mol L^{-1} PB pH 7.0, with and without the presence of H_2O_2, at a scanning rate of 0.1 V·s^{-1}.

2.5. Biosensor reproducibility, repeatability and stability

To evaluate the biosensor reproducibility, cyclic voltammograms were obtained for the same biosensor in three different days. Repeatability was evaluated from 10 consecutive measurements using the same biosensor. To evaluate the biosensor stability, the response of the biosensor was followed every day for 30 days. All analysis were performed with 2×10^{-4} mol L^{-1} peroxide solution in 0.1 mol L^{-1} PB (pH 7.0) at a scan rate of 0.1 V·s^{-1}. After each measurement, the biosensor was stored in 0.1 M PB at 4 °C.

2.6. Analytical curve

Chronoamperometry was used to obtain the biosensor analytical curve, through consecutive additions of 20 μL of 0.02 mol L^{-1} H_2O_2

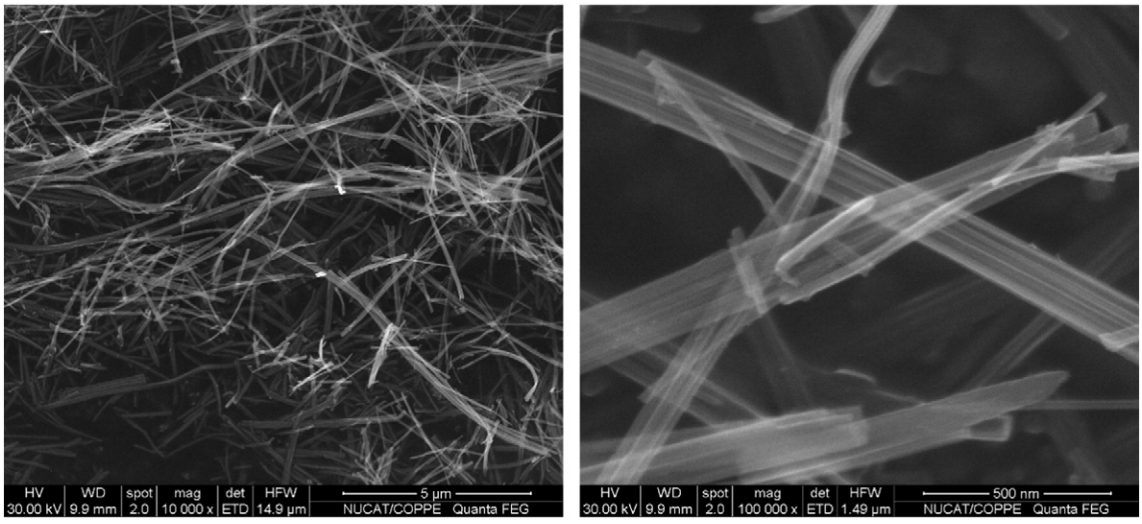

Fig. 1. FEG/SEM micrographs of synthesized of titanate nanowires (TNW).

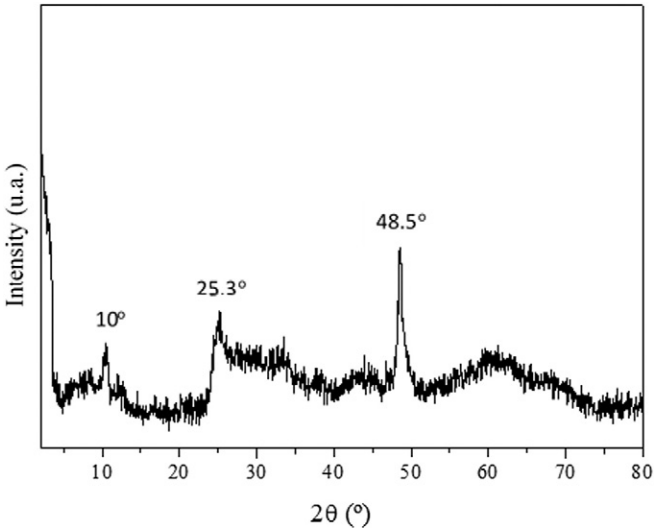

Fig. 2. XRD patterns of synthesized TNW.

solution in 0.1 M PB pH 7.0, under magnetic stirring. A potential of −0.98 V (*vs* Ag electrode) was chose for this test, based on CV measurements. The analytical curve was obtained by representing the average reduction current as a function of the H_2O_2 concentration. The detection limit (DL) and the quantification limit (QL) were calculated from Eqs. (1) and (2), respectively [37]:

$$DL = \frac{3\,\sigma_a}{CS} \quad (1)$$

$$QL = \frac{10\,\sigma_a}{CS} \quad (2)$$

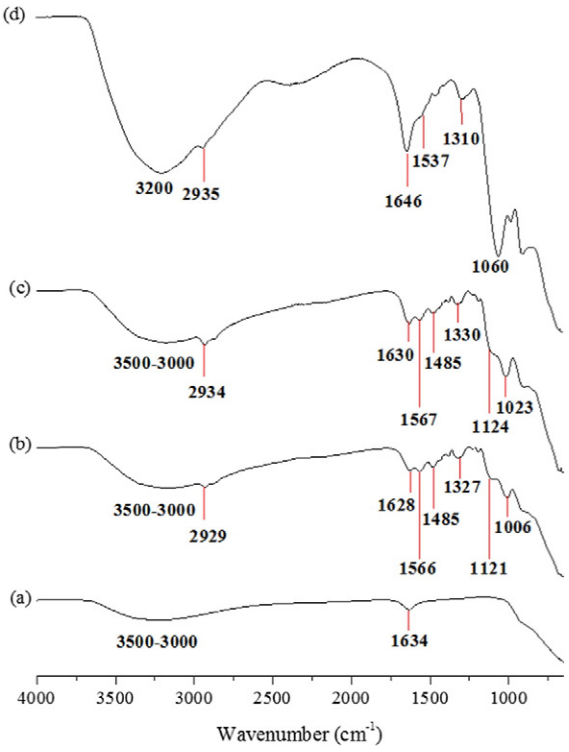

Fig. 4. FTIR spectra of (a) TNW, (b) TNW/APTMS, (c) TNW/APTMS/GLU, (d) TNW/APTMS/GLU/HRP.

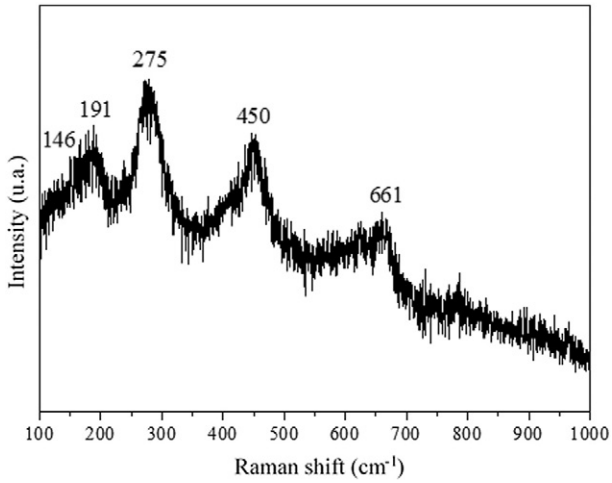

Fig. 3. Raman spectrum of synthesized TNW.

Where CS is the slope of the regression line and σ_a is the standard deviation of the linear coefficient.

3. Results and discussion

3.1. Titanate nanowires characterization

The morphology of the synthesized titanate nanostructures was analysed through scanning electron microscopy (FEG/SEM). As can be seen in Fig. 1, nanowires with diameter of about 20 nm were obtained. The specific area was 177 m^2/g, as determined by N_2 physisorption, which is consistent with nanowire morphology.

Diffractogram of TNW is shown in Fig. 2. The diffraction lines are narrow and intense, indicating that the crystallites have a regular crystal lattice and a size that is relatively large compared to the wavelength of the X-rays. The peak at $2\theta = 10°$ is typical of lamellar titanates and can be attributed to the interlayer distance in the structure $Na_xH_{2-x}Ti_3O_7.nH_2O$. This peak is also related to the presence of sodium in the structure, as the presence of the sodium increases the distance between the layers [38]. A reduction in the peak intensity at 10° is expected as Na^+ cations are exchanged for H^+. Peaks at $2\theta = 25.3°$ and 48.5° corresponds to the anatase phase [38].

Raman spectrum, in Fig. 3, show bands at 661 cm^{-1}, 450 cm^{-1} and 275 cm^{-1} assigned to Ti—O symmetric stretching, Ti—O—Ti vibrations and Ti—O bond, respectively [39]. The bands at 191 cm^{-1} and

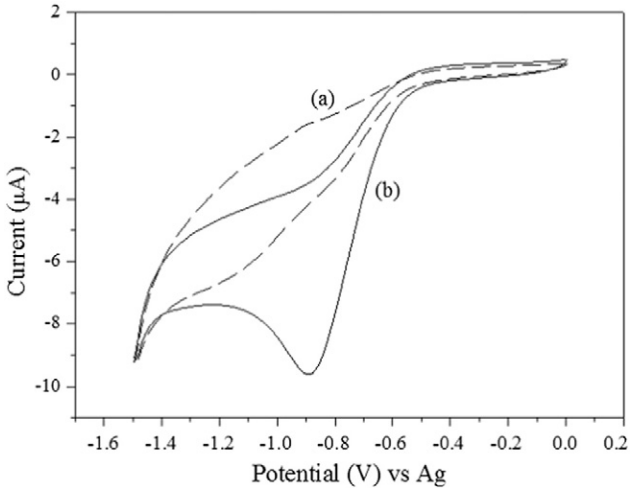

Fig. 5. Cyclic voltammograms for the bare screen-printed electrode (a) and for the biosensor (b) in 0.1 mol L^{-1} phosphate buffer (pH 7), scanning rate of 0.1 $V \cdot s^{-1}$.

Table 2
Comparison of HRP immobilization through different strategies.

Support	Enzyme coverage (mg_{HRP}/m^2)	Enzyme coverage ($moléculas_{HRP}/cm^2$)	Reference
TNW/APTMS/GLU	1.62	2.21×10^{12}	This work
TNW	1.70	2.41×10^{12}	[20]
TNW/APTMS/BQ	1.05	1.43×10^{12}	[42]
Mesoporous silica	0.076	2.11×10^{12}	[45]
Au	–	2.0×10^{12}	[46]
Diamond nanocrystals	–	7.3×10^{13}	[47]

TNW: titanate nanowires; APTMS: 3-(aminopropyl)trimethoxysilane; GLU: glutaraldehyde; EDC: 1-ethyl-3-(3-dimethylaminopropyl)carbodiimide; NHS: N-hydroxysuccinimide; BQ: 1,4-Benzoquinone.

146 cm^{-1} are characteristics for *A*1g and Eg mode, respectively, of anatase TiO_2. According to Gajović et al. [40] in the case of nanotubes obtained from anatase precursor, above determined temperature, titanate nanotubes in H-form, $H_2Ti_3O_7$, can be transformed to anatase, while Na-form, $Na_2Ti_3O_7$, showed phase transition to hexatitanate nanowires. Bands related to the presence of sodium in the structure, at 1063 cm^{-1} (Ti—O—Na stretching) and at 910 cm^{-1} (Ti—O—Na interlayer) are not evident. Fluorescence X-ray (data not shown) also indicates the replacement of Na^+ for H^+ in the structure, confirming the formation of protonic titanates, with purity superior to 99%.

3.2. HRP immobilization on TNW

The strategy for immobilization of HRP on TNW through covalent bond was evaluated by FTIR (Fig. 4). Fig. 4a show the spectrum of bare TNW, which presents bands in the range of 3500–3000 cm^{-1}, related to the presence of surface OH groups (broad band) and at 1630 cm^{-1}, characteristics of angular deformation of the groups in water molecule [41].

The reaction with APTMS (Fig. 4b) was confirmed by the appearance of the bands at 1120 cm^{-1} and 907 cm^{-1}, attributed to the presence of Si—O—Si and Si—OH bonds, respectively. At the same time, the bands around 2930 cm^{-1} (asymmetrical stretching) and between 1500 cm^{-1} and 1300 cm^{-1} (symmetric and asymmetric angular deformation) are characteristics of the methylene groups present in the segment 3-aminopropyl. The presence of the amino groups are suggested by the bands at 1510 cm^{-1} (angular deformation of the NH bond by the presence of NH_3^+ or hydrogen bound to NH_2) and at 1225 cm^{-1} (axial deformation of the C—N bond) [41–42].

After reaction with glutaraldehyde (Fig. 4c), the loss of amino groups and coupling of C═N was confirmed by the decreases of the bands at 1510 cm^{-1} and 1223 cm^{-1}. The higher intensity of the band around 1630 cm^{-1} is related to the appearance of C═N groups [41].

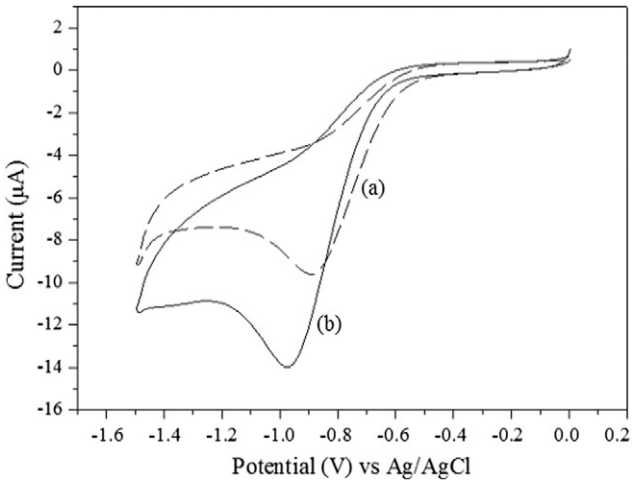

Fig. 6. Cyclic voltammograms for the biosensor in 1 mol L^{-1} phosphate buffer (pH 7) without H_2O_2 (a) and in the presence of 2 × 10–^{4} mol L^{-1} de H_2O_2 (b).

Upon HRP adsorption (Fig. 4d), the appearance of new bands at 1646 cm^{-1}, 1537 cm^{-1} and 1310 cm^{-1} is assigned to the groups —CONH— (amide I), —CN— stretching (amide III) and amide II, respectively. The increased bandwidth around 1060 cm^{-1} is characteristics of —CO— bond stretch [43]. These results confirm that HRP was successfully immobilized onto TNW by covalent coupling through amine groups.

Although the functionalization improves the reactivity of the surface, TNW has become more aggregated, reducing its specific surface from 177 m^2/g to 22 m^2/g after reaction with glutaraldehyde. Sovic et al. (2011) also reported a 50% decrease in specific surface of titanate nanotubes after functionalization with APTMS [42].

The estimated amount of immobilized enzyme was 1.62 ± 0.46 mg HRP/m^2. As HRP molecular weight is about 44 kDa [44], an estimative for the surface coverage was 2.21×10^{12} molecules/cm^2. Table 2 compares the results obtained in this work with key studies in the literature.

Specific activity of immobilized HRP was 490 ± 35 U·mg^{-1}, while free HRP exhibited a specific enzyme activity of 1014 ± 150 U·mg^{-1}. This result shows that, after immobilization, the enzyme retains about 48% of its specific activity. Camaroni et al. [48] reported a loss of 60% of activity upon immobilization of HRP. The residual enzyme activity was also recorded as a function of storage time for both free and immobilized HRP, stored in 0.1 mol L^{-1} PB (pH 7) at 4 °C. Compared to free HRP, immobilized HRP maintains 56% of its initial activity after 120 days of storage. For the same period, free HRP has preserved only 25% of its initial activity.

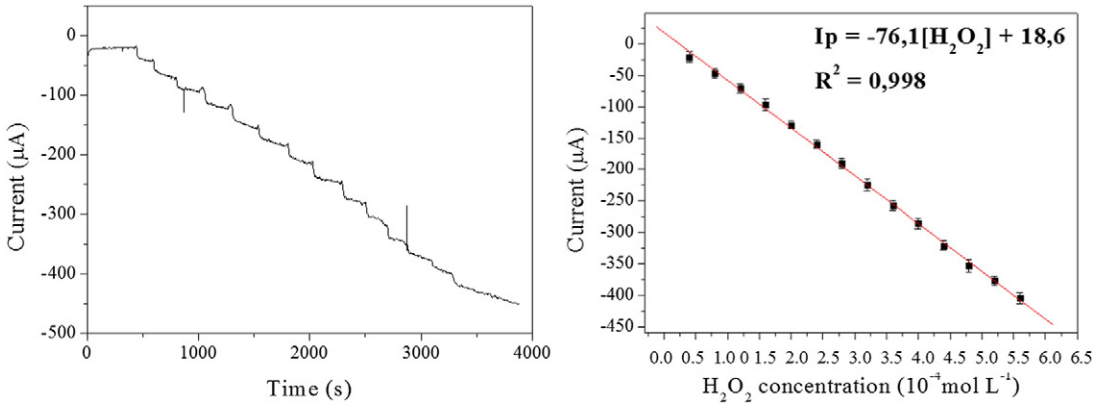

Fig. 7. Biosensor amperometric response to successive addition of 20 μL of 0.02 mol L^{-1} H_2O_2 at a potential of −0.98 V (a). Biosensor analytical curve at the same potential (b).

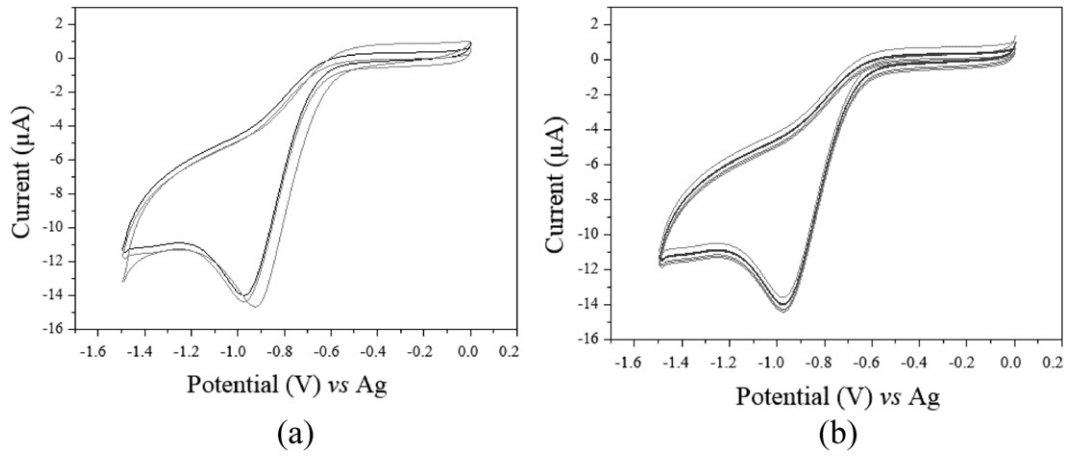

Fig. 8. Reproducibility (a) and repeatability (b) of the biosensor in 0.1 mol L^{-1} phosphate buffer (pH 7) in the presence of 2×10^{-4} mol L^{-1} H_2O_2.

3.3. Electrochemical characterizations

Screen-printed electrodes modified through deposition of HRP-containing TNW were characterized by cyclic voltammetry in 0.1 mol L^{-1} phosphate buffer (pH 7) in the range from 0 to −1.5 V, at a scan rate of 0.1 $V \cdot s^{-1}$. As shown in Fig. 5, no redox peaks were observed for the bare electrode (a), demonstrating that it is not electroactive in this potential range. For the modified electrode, a cathodic peak is seen at about −0.88 V (*vs* Ag) which is attributed to the presence of the HRP electroactive center.

The performance of the biosensor towards the electrochemical reduction of H_2O_2 is seen in Fig. 6. In the presence of peroxide, the reduction peak current is increased and has a shift to a more negative potential (−0.98 V), indicating that immobilized HRP is responsible for H_2O_2 biocatalytic reduction. These results confirm that TNW are a suitable matrix for HRP immobilization for application in biosensing. Nicolini et al. [23] also reported a good performance of carbon paste electrodes containing HRP immobilized in TNW.

3.4. Analytical performances of the biosensor

The amperometric response of the biosensor to successive additions of 20 μL of a 0.02 mol L^{-1} H_2O_2 solution at a potential of −0.98 V (*vs* Ag) was evaluated (Fig. 7a) and the corresponding analytical curve of the biosensor is shown in Fig. 7b. The response was linear in the range of 40 to 560 μmol L^{-1}, with a correlation coefficient of 0.9980. Detection limit (DL) was 10.7 ± 0.01 μmol L^{-1}, which is similar to the DL reported in other studies in the literature [49–50]. Quantification limit (QL) was 35.6 μmol L^{-1}. The biosensor response time – elapsed time to achieve the current peak upon H_2O_2 addition – was 15 s.

Reproducibility was evaluated using three different fabricated biosensors (Fig. 8a). The measurements RSD (relative standard deviation) was as low as 4.7%. Repeatability was evaluated through 10 successive measurements using the same biosensor (Fig. 8b). In this case, RSD was 3.3%. Similar results of were obtained by other nanostructured biosensors for detection of H_2O_2 reported in the literature [51–52].

Biosensor stability during storage in 0.1 mol L^{-1} PB (pH 7.0) at 4 °C was evaluated. The cathodic current after 15 days was 92% of the initial value; after 30 days, a reduction of 50% in the current was observed. The good stability of the biosensor is attributed to the covalent immobilization and to the favorable microenvironment propitiated by the TNW, which minimizes enzyme losses, assuring the appropriate performance of the biosensor. These results confirm that the method for HRP immobilization is a key factor in biosensors research. Table 3 summarizes the performance of selected biosensors for peroxide detection based on screen-printed carbon electrodes.

4. Conclusions

In this work we show that the covalent immobilization of HRP enzyme on titanate nanowires constitutes a good platform for manufacture of peroxide biosensors. HRP denaturation was minimized upon immobilization and the enzyme electrocatalytic activity was preserved. The modification of screen-printed electrodes with HRP-containing TNW was a very successful strategy. The biosensor presented a low reduction potential for H_2O_2, around −0.98 (V *vs* Ag), and detection limit of 10.7 μmol L^{-1} in the linear range of 40 to 560 μmol L^{-1}. In addition, the biosensor presented good reproducibility, repeatability and stability to storage.

Table 3
Biosensors based on carbon screen-printed electrodes for H_2O_2 detection.

Biosensor	E (V *vs* Ag/AgCl)	Linear range (μmol l^{-1})	Limit of detection (μmol l^{-1})	Sensitivity[a] (μA mM^{-1})	Stability % response (days)	Reference
TNW/APTMS/GLU/HRP	−0.4	40–560	10.7	7.6	92% (15)	This work
HRP	0	10–250	–	–	–	[30]
CHIT/NpAu/HRP	−0.40	10–11,300	0.65	–	95% (30)	[33]
RGO-HRP	−0.26	9–195	–	17.6	–	[34]
GS–Nafion/Fe_3O_4-Au-HRP	−0.30	20–2,500	12	4.8	90% (28)	[35]
THI/GLU/HRP	–	5–65	0.50	–	92% (30)	[53]
Au/HRP	−0.34	0.8–1000	0.40	27.6	90% (30)	[54]
Nafion/HRP	−0.33[b]	5.98–35.36	0.48	14.3	95% (30)	[31]
Au/Hb	−0.23[b]	10–320	5.50	–	90% (30)	[32]

TNW – titanate nanowires; GLU – glutaraldehyde; GS – graphene sheet; RGO – reduced graphene oxide; CHIT – Chitosan; NpAu – Golden nanoparticles; THI - thionine; Hb – Hemoglobin.
[a] The sensitivity was determined from the analytical curve and indicates how the signal changes when the analyte concentration changes.
[b] Reduction potential *vs* saturated calomel electrode (SCE).

References

[1] A.P.F. Turner, Biosensors: sense and sensibility, Chem. Soc. Rev. 42 (2013) 3184–3196.
[2] W. Chen, S. Cai, Q.Q. Ren, W. Wen, Y. Zhao, Recent advances in electrochemical sensing for hydrogen peroxide: a review, Analyst 137 (2012) 49–58.
[3] Y. Luo, H. Liu, Q. Rui, Y. Tian, Detection of extracellular H_2O_2 released from human liver cancer cells based on TiO_2 nanoneedles with enhanced electron transfer of cytochrome C, Anal. Chem. 81 (2009) 3035–3041.
[4] M.Y. Hua, H.C. Chen, C.K. Chuang, R.Y. Tsai, J.L. Jeng, H. Yang, Y.T. Chern, The intrinsic redox reactions of polyamic acid derivatives and their application in hydrogen peroxide sensor, Biomaterials 32 (2011) 4885–4895.
[5] K. Zhou, Y. Zhu, X. Yang, J. Luo, C. Li, S. Luan, A novel hydrogen peroxide biosensor based on Au–graphene–HRP–chitosan biocomposites, Electrochim. Acta 55 (2010) 3055–3060.
[6] M.K. Bojdi, M.H. Mashhadizadeh, M. Behbahani, A. Farahani, S.S.H. Davarani, A. Bagheri, Synthesis, characterization and application of novel lead imprinted polymer nanoparticles as a high selective electrochemical sensor for ultra-trace determination of lead ions in complex matrixes, Electrochim. Acta 136 (2014) 59–65.
[7] H. Hosseini, M. Behbahani, M. Mahyari, H. Kazerooni, A. Bagheri, A. Shaabani, Ordered carbohydrate-derived porous carbons immobilized gold nanoparticles as a new electrode material for electrocatalytical oxidation and determination of nicotinamide adenine dinucleotide, Biosens. Bioelectron. 59 (2014) 412–417.
[8] M.K. Bojdi, M. Behbahani, M. Najafi, A. Bagheri, F. Omidi, S. Salimi, Selective and sensitive determination of uranyl ions in complex matrices by ion imprinted polymers-based electrochemical sensor, Electroanalysis 27 (2015) 2458–2467.
[9] M.K. Bojdi, M. Behbahani, G. Hesam, M.H. Mashhadizadeh, Application of magnetic lamotrigine-imprinted polymer nanoparticles as an electrochemical sensor for trace determination of lamotrigine in biological samples, RSC Adv. 6 (2016) 32374–32380.
[10] W. Ashok Mulchandani, N. Myung, Conducting polymer nanowires-based label-free biosensors, Curr. Opin. Biotechnol. 22 (2011) 502–508.
[11] J. Wang, Nanomaterial-based electrochemical biosensors, Analyst 130 (2005) 421–426.
[12] N. Laurent, R. Haddoub, S.L. Flitsch, Enzyme catalysis on solid surfaces, Trends Biotechnol. 26 (2008) 328–337.
[13] J. Wang, L. Wang, J. Di, Y. Tu, Electrodeposition of gold nanoparticles on indium/tin oxide electrode for fabrication of a disposable hydrogen peroxide biosensor, Talanta 77 (2009) 1454–1459.
[14] H. Xue, W. Sun, B. He, Z. Shen, Single-wall carbon nanotubes as immobilization material for glucose biosensor, Synth. Met. 135 (2003) 831–832.
[15] J. Wang, M. Musameh, Carbon-nanotubes doped polypyrrole glucose biosensor, Anal. Chim. Acta 539 (2005) 209–213.
[16] K. Thandavan, S. Gandhi, N. Nesakumar, S. Sethuraman, J.B.B. Rayappan, U.M. Krishnan, Hydrogen peroxide biosensor utilizing a hybrid nano-interface of iron oxide nanoparticles and carbon nanotubes to assess the quality of milk, Sensors Actuators B (2015) 166–173.
[17] W.N. Liu, D. Ding, Z.L. Song, X. Bian, X.K. Nie, X.B. Zhang, Z. Chen, W. Tan, Hollow graphitic nanocapsules as efficient electrode materials for sensitive hydrogen peroxide detection, Biosens. Bioelectron. 52 (2014) 438–444.
[18] H. Tokudome, M. Miyauchi, Electrochromism of titanate-based nanotubes, Angew. Chem. Int. Ed. 44 (2005) 1974–1977.
[19] Z. Liu, X. Zhang, S. Nishimoto, M. Jin, D.A. Tryk, T. Murakami, A. Fujishima, Anatase TiO_2 nanoparticles on rutile TiO_2 nanorods: a heterogeneous nanostructure via layer-by-layer assembly, Langmuir 23 (2007) 10916–10919.
[20] J.V. Nicolini, N.M. Resende, H.C. Ferraz, Adsorption of horseradish peroxidase onto titanate nanowires, J. Chem. Technol. Biotechnol. 90 (2014) 739–746.
[21] S. Mathur, A. Erdem, C. Cavelius, S. Barth, J. Altmayer, Amplified electrochemical DNA-sensing of nanostructured metal oxide films deposited on disposable graphite electrodes functionalized by chemical vapor deposition, Sensors Actuators B 136 (2009) 432–437.
[22] J. Qiu, S. Zhang, H. Zhao, Recent applications of TiO_2 nanomaterials in chemical sensing in aqueous media, Sensors Actuators B 160 (2011) 875–890.
[23] J.V. Nicolini, H.C. Ferraz, N.S. Resende, Immobilization of horseradish peroxidase on titanate nanowires for biosensing application, J. Appl. Electrochem. 46 (2016) 17–25.
[24] H. Tang, F. Yan, Q. Tai, H.L.W. Chan, The improvement of glucose bioelectrocatalytic properties of platinum electrodes modified with electrospun TiO_2 nanofibers, Biosens. Bioelectron. 25 (2010) 1646–1651.
[25] X. Liu, H. Feng, R. Zhao, Y. Wang, X. Liu, A novel approach to construct a horseradish peroxidase hydrophilic ionic liquids|Au nanoparticles dotted titanate nanotubes biosensor for amperometric sensing of hydrogen peroxide, Biosens. Bioelectron. 31 (2012) 101–104.
[26] P. Xiao, B.B. Garcia, Q. Guo, D. Liu, G. Cao, TiO_2 nanotube arrays fabricated by anodization in different electrolytes for biosensing, Electrochem. Commun. 9 (2007) 2441–2447.
[27] P. Benvenuto, A.K.M. Kafi, A. Chen, High performance glucose biosensor based on the immobilization of glucose oxidase onto modified titania nanotube arrays, J. Electroanal. Chem. 627 (2009) 76–81.
[28] P. Luo, G. Xie, Y. Liu, H. Xu, S. Deng, F. Song, Electrochemical detection of blood alcohol concentration using a disposable biosensor based on screen-printed electrode modified with Nafion and gold nanoparticles, Clin. Chem. Lab. Med. 46 (2008) 1641–1647.
[29] M. Li, Y.T. Li, D.W. Li, Y.T. Long, Recent developments and applications of screen-printed electrodes in environmental assays-a review, Anal. Chim. Acta 734 (2012) 31–44.
[30] S. Ledru, N. Ruillé, M. Boujtita, One-step screen-printed electrode modified in its bulk with HRP based on direct electron transfer for hydrogen peroxide detection in flow injection mode, Biosens. Bioelectron. 21 (2006) 1591–1598.
[31] Y.J. Teng, S.H. Zuo, M.B. Lan, Direct electron transfer of horseradish peroxidase on porous structure of screen-printed electrode, Biosens. Bioelectron. 24 (2009) 1353–1357.
[32] X. Xu, S. Liu, H. Ju, Disposable biosensor based on a hemoglobin colloidal gold-modified screen-printed electrode for determination of hydrogen peroxide, IEEE Sensors J. 4 (2004) 390–394.
[33] T. Tangkuaram, C. Ponchio, T. Kangkasomboon, K. Panadda, V. Waret, Design and development of a highly stable hydrogen peroxide biosensor on screen printed carbon electrode based on horseradish peroxidase bound with gold nanoparticles in the matrix of chitosan, Biosens. Bioelectron. 22 (2007) 2071–2078.
[34] S. Palanisamy, B. Unnikrishnan, S.M. Chen, An amperometric biosensor based on direct immobilization of horseradish peroxidase on electrochemically reduced graphene oxide modified screen printed carbon electrode, Int. J. Electrochem. Sci. 7 (2012) 7935–7947.
[35] Y. Xin, X. Fu, L. Hong, A novel H_2O_2 biosensor based on Fe_3O_4–Au magnetic nanoparticles coated horseradish peroxidase and graphene sheets–Nafion film modified screen-printed carbon electrode, Electrochim. Acta 109 (2013) 750–755.
[36] T. Kasuga, M. Hiramatsu, A. Hoson, T. Sekino, K. Niihara, Titania nanotubes prepared by chemical processing, Adv. Mater. 11 (1999) 1307–1311.
[37] R. Ismail, H.Y. Lee, N.A. Mahyudin, F.A. Bakar, Linearity study on detection and quantification limits for the determination of avermectins using linear regression, J. Food Drug Anal. 22 (2014) 407–412.
[38] E. Morgado Jr., M.A.S. Abreu, G.T. Moure, B.A. Marinkovic, P.M. Jardim, A.S. Araujo, Effects of thermal treatment of nanostructured trititanates on their crystallographic and textural properties, Mater. Res. Bull. 42 (2007) 1748–1760.
[39] A. Turki, H. Kochkar, C. Guillard, G. Berhault, A. Ghorbel, Effect of Na content and thermal treatment of titanate nanotubes on the photocatalytic degradation of formic acid, Appl. Catal. B Environ. 138-139 (2013) 401–415.
[40] A. Gajović, I. Friščić, M. Plodinec, D. Iveković, High temperature Raman spectroscopy of titanate nanotubes, J. Mol. Struct. 924–926 (2009) 183–191.
[41] R.M. Silverstein, F.X. Webster, D. Kiemle, Spectrometric Identification of Organic Compounds, John Wiley & Sons, New York, 2005.
[42] D. Sovic, A. Gajovic, D. Ivekovic, Bioelectrocatalytic and biosensing properties of horseradish peroxidase covalently immobilized on (3-aminopropyl) trimethoxysilane-modified titanate nanotubes, Electrochim. Acta 56 (2011) 9953–9960.
[43] M. Monier, D.M. Ayad, Y. Wei, A.A. Sarhan, Immobilization of horseradish peroxidase on modified chitosan beads, Int. J. Biol. Macromol. 46 (2010) 324–330.
[44] W. Kg, Amino acid sequence studies of horseradish peroxidase. Amino and carboxyl termini, cyanogen bromide and tryptic fragments, the complete sequence, and some structural characteristics of horseradish peroxidase C, Eur. J. Biochem. 96 (1979) 483–502.
[45] M. Wan, W. Lin, L. Gao, H. Gu, J. Zhu, Promoting immobilization and catalytic activity of horseradish peroxidase on mesoporous silica through templatemicelles, J. Colloid Interface Sci. 377 (2012) 497–503.
[46] A.E. Radi, X. Muñoz-Berbel, M. Cortina-Puig, J.L. Marty, Novel protocol for covalent immobilization of horseradish peroxidase on gold electrode surface, Electroanalysis 21 (2009) 696–700.
[47] Q. Wang, A. Kromka, J. Houdkova, O. Babchenko, B. Rezek, M. Li, B. Boukherroub, S. Szunerits, Nanomolar hydrogen peroxide detection using horseradish peroxidase covalently linked to undoped nanocrystalline diamond surfaces, Langmuir 28 (2012) (587-59).
[48] S.S. Camaroni, K.F. Fernandes, Covalent immobilization of horseradish peroxidase onto poly(ethylene terephthalate)-poly(aniline) composite, Process Biochem. 39 (2004) 883–888.
[49] W.G. Kafi Akm, A. Chen, A novel hydrogen peroxide biosensor based on the immobilization of horseradish peroxidase onto Au-modified titanium dioxide nanotube arrays, Biosens. Bioelectron. 24 (2008) (566–57).
[50] Z. Li, X. Cui, J. Zheng, Effects of microstructure of carbon nanofibers for amperometric detection of hydrogen peroxide, Anal. Chim. Acta 597 (2007) 238–244.
[51] N. Wei, X. Xin, J. Du, J. Li, A novel hydrogen peroxide biosensor based on the immobilization of hemoglobin on threedimensionally ordered macroporous (3DOM) gold-nanoparticledoped titanium dioxide (GTD) film, Biosens. Bioelectron. 26 (2011) 3602–3607.
[52] A. Sassolas, L.J. Blum, B.D.L. Bouvier, Immobilization strategies to develop enzymatic biosensors, Biotechnol. Adv. 30 (3) (2012) 489–511.
[53] Q. Gao, F. Yang, Y. Ma, X. Yang, The modification of screen-printed carbon electrodes with amino group and its application to construct a H_2O_2 biosensor, Electroanalysis 16 (2004) 730–735.
[54] H. Ju, X. Xu, S. Liu, A novel hydrogen peroxide sensor via the direct electrochemistry of horseradish peroxidase immobilized on colloidal gold modified screen-printed electrode, Sensors 3 (2003) 350–360.